Journal of Materials and Electronic Devices 1 (2020) 32-44

Improvement of Surface Properties of Pure Iron Modified by Novel Plasma Electrolytic Oxy-Carburising Technique

Levent Cenk Kumruoglu

University of Cumhuriyet, Engineering Faculty, Metallurgy and Materials Eng. Dept., Campus-Sivas, Turkey

Plasma electrolytic oxy-carburising of pure iron was carried out by using novel plasma electrolysis technique using dynamic electrolyte flow between substrate and electrolytes. The electrolytes contained glycerine and sodium carbonate as a carbon source and conductivity provider, respectively. This novel plasma electrolysis (PE) technique and nozlle setup can provide high wear and corrosion resistance due to the high diffusion rate of O and C into the metal surface, and subsequent quenching results in the formation of multi-phase combinations of carbo-oxides, including mixtures of (Fe)2-3O3-4, austenite, martensite, (Fe)xC and a nanocrystalline layer. The samples were treated for 1–5 minutes at voltages varying from 200 to 350 V. Constituent phases, surface morphology and topography, elemental analysis, microstructure and mechanical property investigations were conducted by XRD, OM and SEM, EDS, profilometry and microhardness testing, respectively. Potentiodynamic polarization measurements were carried out to determine the corrosion resistance of the oxy-carburised samples. The new PE technique was found to provide a more controllable process and better surface properties than conventional PEs.. The optimum process parameter was assessed at 300 V. An oxy-carburized layer of 30µm thickness was obtained, which had a hardness of 820 HV over 5 minutes at 300 V. Compared to untreated pure iron (-0.68 V), a more positive corrosion potential (-0.57 V) was obtained for the oxy-carburized layers.

Keywords: Plasma electrolytic oxy-carburising, Iron, Hardness, Wear Test, Corrosion

Submission Date: 27 January 2020
Acceptance Date: 08 April 2020

Corresponding author: lkumru@cumhuriyet.edu.tr (Levent Cenk Kumruoglu), Tel/Fax +903462191010/2494

1. Introduction

As a rule, among all the thermo-chemical diffusion processes, elements such as carbon, nitrogen and boron are diffused into metal surfaces at elevated temperatures to improve the surface properties and the strength of metallic substrates [1]. Carburising is one of the most common thermo-chemical diffusion processes and it can be performed on metallic materials by diffusion of carbon atoms into the iron or steel surfaces that have low carbon contents. Carburising alters the chemical composition of the surface of a low-carbon steel component, so that subsequent fast cooling, by “quenching”, produces a hard “case” combined with a softer/tougher “core” [2]. Plasma Electrolysis (PE)) is an electro-thermo-chemical diffusion/saturation treatment, usually conducted at elevated temperatures in a liquid state containing interstitial elements [3, 4]. So far, the plasma electrolytic carburising technique has been performed on several engineering materials such as titanium [3, 5], low carbon steel [6], low alloyed steel [7], and ferrous metals [8, 9]. Even though a wide range of materials have been treated using the plasma electrolytic carburising technique, there is no published study dealing with the problem of corrosion and wear resistance of oxy-carburised pure iron. Therefore, the corrosion and wear behaviour of oxy-carburised pure iron are not yet clear. Controlling the temperature and edge melting of the

samples is a major problem in carburising with EP. In this study, oxy-carburising process was applied without immersion in electrolyte and temperature was measured by infrared pyrometer. The temperature value was kept at austenite temperature (900 °C) with 5 °C degree precision and prevented melting of sample edges. In order to evaluate the wear behaviour of the oxy-carburised layer under different contact conditions, dry reciprocating sliding tests were conducted in this work. The salt-water corrosion behaviour of plasma electrolytic oxy-carburised surface was evaluated by means of potentiodynamic polarization scans, open circuit potential measurements, and electrochemical impedance spectroscopy. characteristics.

2.- Experimental Studies

Testing coupons (15x25x1.5 mm) were made from pure iron (99.97% weight) as the substrate material. Prior to PE, the substrates were mechanically polished to achieve a surface finish of Ra ≈ 0.15 µm, then ultrasonically cleaned in ethanol for 5 minutes and dried with hot air steam. The exact composition of electrolytes can be altered to the substrate metal involved, and the desired properties of the saturation can be obtained [4]. Therefore, solutions of glycerine (30% C3H5(OH)3), sodium carbonate (Na2CO3 12%) and H2O2 in distilled water were used as electrolytes. Glycerine as a carbon source has the decomposition products of Hydrogen (H2), Carbon monoxide (CO) and Carbon dioxide (CO2) [10], which principally promotes carbon diffusion. H2O2 as a hydrogen and oxygen which principally promotes oxygen diffusion to increase stable oxy-carbure phase. PE was carried out on a specially designed and instrumented rig, a photograph of treatment was shown in Figure 1. In the Novel EP system, a 316L quality diffuser was placed in a nozzle. With the aid of a pump, the electrolyte was continuously pumped to contact the bottom surface of the sample placed above the nozzle. Thus, the current density per unit area was taken under control. The flow of electrolyte in contact with the sample was controlled by flowmeter. After the electrolyte came into contact with the sample and formed the plasma, it was conveyed back to the electrolyte tank by gravity and pumped back to the sample. In this way, the differences in composition at the sample-electrolyte interface and the melting due to excessive temperature rise were avoided. The circulation of the electrolyte and the elements C, H, O were maintained at the same level and diffusion rates and temperature did not change during the process. In a PE process, the surface characteristics can be modified via processing variables, such as the potential, electrolyte composition, temperature, and current density [4, 11]. The temperature of the electrolyte is one of the most important parameters in PE. In order to begin the plasma rapidly and to get a continuous plasma envelope form, the electrolyte temperature was adjusted to 85◦C. At this temperature, the plasma stabilization on the cathode surface becomes easier, otherwise the current fluctuations are large and difficult to stabilize [12]. The oxy-carburising temperature of the sample was controlled by both an infrared pyrometer and a K type contact thermocouple. The samples were heated and held at 900 °C throughout the PE treatment. Pure Iron coupons are not immersed in the electrolyte, but placed on a continuously circulated electrolyte in a special PE system. The electrolyte was pumped to provide a continuous flow out of a nozzle. Only the bottom surface of the sample placed on the nozzle came into contact with the electrolyte, and plasma was formed only at the electrolyte sample interface. Thus, the sample temperature was accurately measured from the upper surface with a pyrometer. Continuous circulation of the electrolyte kept the oxygen level and the carbon level at the electrolyte-sample interface. The electrical bias was provided by a high-voltage DC power supply rated at 30 kW. The substrates were conducted cathodically and treated for 1–5 minutes at voltages varying from 200 to 350V. Subsequently, oxy-carburised samples were quenched in the same electrolyte by switching off the power source. Through quenching, the carbon diffused into the pure iron lattice structure turned into a martensitic structure on the sample surface. For each new sample, current and voltage data were recorded via an acquisition system to find out the optimum process parameters.

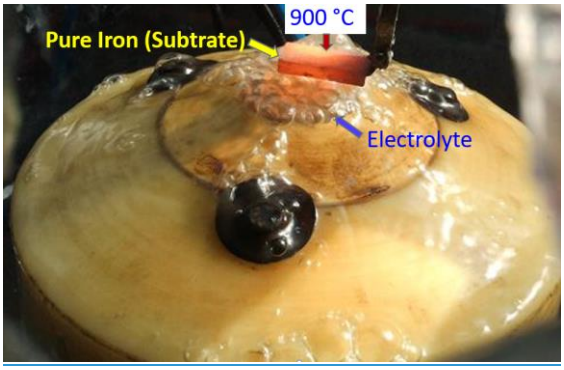

Figure 1: *A photograph of the PE oxy-carburising at 900 °C*

A reciprocating dry sliding wear test was implemented to assess the wear resistance of oxy-carburized layers formed on the pure iron substrates against a 10 mm diameter AISI 52100 steel ball [13]. The following parameters were selected: normal load: 5 N, 10N, 15N; track length: 10 mm; frequency: 5 Hz; sliding speed: 0.1 ms−1; sliding

distance 180, 360 and 540 m; atmosphere: ambient air (18±2 °C, 20–30% humidity). Before and after each test, both the samples and the AISI 52100 steel ball were cleaned ultrasonically in acetone and then dried.

A JEOL-6060LV scanning electron microscopy (SEM), glow discharge-optical emission spectroscopy (GD-OES) and optical microscopy were used to observe the microstructure of the samples to study the surface morphology of oxy-carburized layers. The morphology of each wear scar was observed by stereo microscopy and a 2D surface profilometer using a Dektak3ST surface profilometer fitted with a 12.5μm radius stylus and 3mg contact force. EDS was used to collect information regarding the chemical composition of the wear debris. The microstructure and phase composition of oxy-carburised layers were investigated by means of a Siemens D5000 X-ray diffractometer (XRD) with CuKα radiation. A Glancing Angle XRD technique was also performed to identify the diffraction pattern of thin films, with a minimum contribution from the pure iron substrate. The used tube acceleration voltage and current were of 40 kV and 30 mA, respectively. A Leica VHMT MOT microhardness tester was used with a 25 g load to measure hardness of substrate.

The corrosion performance of the oxy-carburised samples was studied using Open-Circuit Potential stability measurements (OCP) and potentiodynamic polarization scans. Electrochemical measurements were performed by a Solartron 1286 potentiostat–galvanostat. The electrochemical tests were carried out in an aerated 0.6 M NaCl solution that was prepared according to the ASTM G61 standard procedure [14]. The tests were performed at room temperature and the air was purged into the NaCl solution throughout the corrosion experiment. The polarization voltage swept from about -0.5 V to +1.5 V of open circuit potential at a sweeping rate of 1.167 mV/s SCE; a Pt plate served as a counter electrode. A standard circular surface area (0.738 cm2) of specimen was exposed to the solution. The corrosion current density (Icorr), corrosion potential (Ecorr) and anodic/cathodic Tafel slopes (βa and βc) were calculated from these tests using the CorrWare® software supplied by Scribner Associates

3. Results and discussion

3.1. Structure and morphology characterization

The optimum process parameter was assessed as 300 V for PE experiments. In order to decide this value, several other voltages were applied from 200 V to 350 V. When the applied voltage was 200 V, the majority of this process behaved according to the Faraday rules and a steady state plasma not observed. Monitored and recorded results of performing 250 V were relatively better than the treatment applied at 200 V; nevertheless, the breakdown voltage was not in a steady state mode. For 350 V, even though the characteristics of plasma such as breakdown voltage, bubbling, gas envelope etc. were acceptable, the current fluctuations were large and difficult to stabilize. Furthermore, after biasing 350 V, partial melting zones were observed on the edge of the coupons due to the overheating. The study of determining the ideal voltage for our PE process showed that the optimum voltage was 300 V. The optimum voltage value was determined based on both the most effective plasma stability and the minimum melting and roughness values on the sample surface after PE oxy-carburising. The treatment time may play a significant role on the structure of the saturated layer in terms of environmental concerns, energy consumption, process economy, and the engineering quality of the saturated layer. Therefore, to optimise the influence of the treatment time the samples were oxy-carburised for 1, 3 and 5 minutes at 300 V. It was observed from the treatment time optimisation study that oxy-carburising performed for 5 minutes yielded higher surface hardness and case depth compared to the treatment of 1 and 3 minutes. During PE, the electrolyte levels can decrease, and the saturation kinetics of the process might be affected by this partially consumed precursor that contains elements like C, therefore it is essential to compensate the fading elements in the electrolyte [15]. This problem is sorted by using a large scale electrolyte tank and sensitive flow meters and vapour-phase chromatography, optical emission spectroscopy and a data acquisition system incorporated to regulate the precursor materials' sensitively. As a result, the depletion of C and O elements in an electrolyte during PE was prevented by using a 50 litter electrolyte and circulation pump. The presence of C and O at the sample-electrolyte interface was monitored using optical emission spectroscopy and oscilloscope.

Figure 2 shows the standard deviation of current and voltage as found in the optimization study of process voltage parameters at 200, 250, 300 and 350 V, along with related optical microscopy micrographs taken after the treatments are given. Two different types of approaches were carried out to reveal the PE mechanism on oxy-carburised substrates using electron microscopy. The first route was to occupy standard EDS point and line scan analyses performed on cross-sections of the treated substrate as shown in Figures 3 and 4a. Both figures present

the diffusion of C, O and Fe atoms into the pure iron substrate. Figure 4b, which shows the elemental distributions in the oxy-carburized layer, indicates major elements such as C, O and Fe. Both EDS and GD-OES studies verify the carbon and oxygen diffusion through the base material.

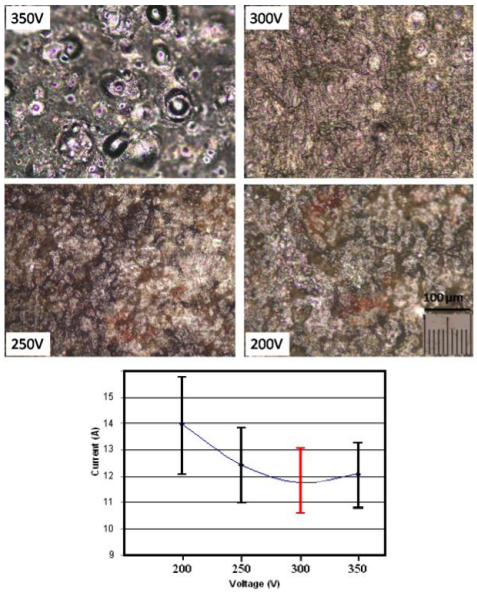

Figure 2*. Current–voltage diagram for PE of pure iron and related OM micrographs taken after treatment*

Two different types of approaches were carried out to reveal the PE mechanism on oxy-carburised substrates using electron microscopy. The first route was to occupy standard EDS point and line scan analyses performed on cross-sections of the treated substrate as shown in Figures 3 and 4a. Both figures present the diffusion of C, O and Fe atoms into the pure iron substrate. Figure 4b, which shows the elemental distributions in the oxy-carburized layer, indicates major elements such as C, O and Fe. Both EDS and GD-OES studies verify the carbon and oxygen diffusion through the base material.

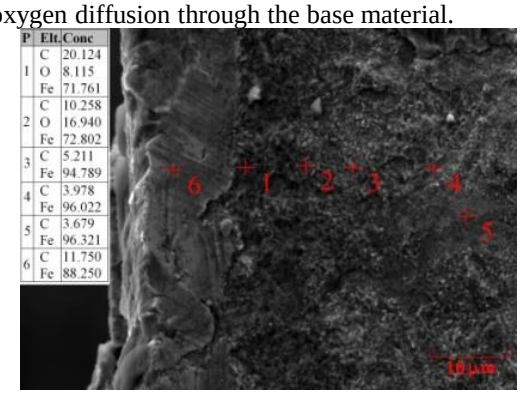

P	Elt.	Conc
1	C	20.124
	O	8.115
	Fe	71.761
2	C	10.258
	O	16.940
	Fe	72.802
3	C	5.211
	Fe	94.789
4	C	3.978
	Fe	96.022
5	C	3.679
	Fe	96.321
6	C	11.750
	Fe	88.250

Figure 3: *Scanning electron microscopy and EDS analyses of cross-section of the treated substrate (300V-5 minutes)*

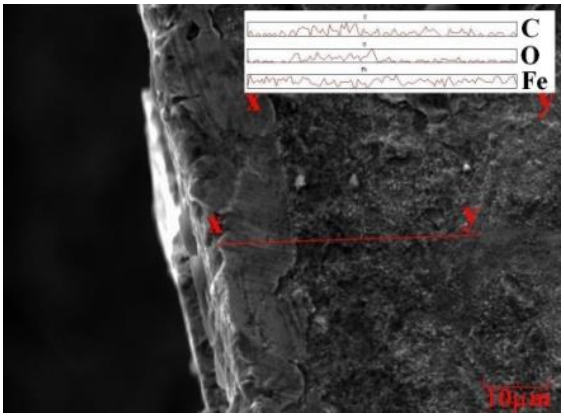

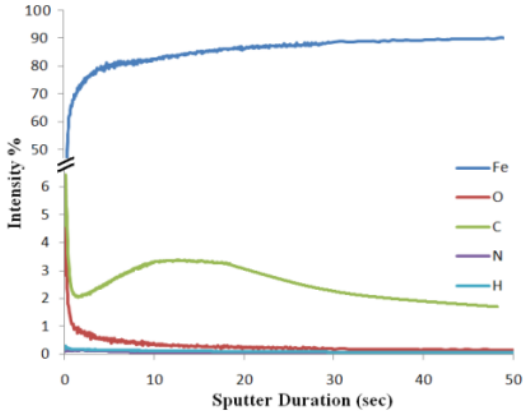

Figure 4: *Line scan SEM-EDS and GD-OES analyses of the treated substrate scanned from surface to core (300V-5 minutes)*

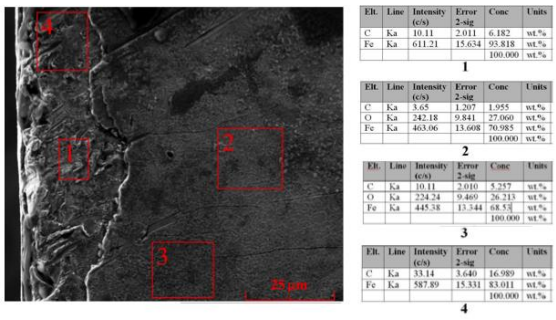

Elt.	Line	Intensity (c/s)	Error 2-sig	Conc	Units
C	Ka	10.11	2.011	6.182	wt.%
Fe	Ka	611.21	15.634	93.818	wt.%
				100.000	wt.%

1

Elt.	Line	Intensity (c/s)	Error 2-sig	Conc	Units
C	Ka	3.65	1.207	1.955	wt.%
O	Ka	242.18	9.841	27.060	wt.%
Fe	Ka	463.06	13.608	70.985	wt.%
				100.000	wt.%

2

Elt.	Line	Intensity (c/s)	Error 2-sig	Conc	Units
C	Ka	10.11	2.010	5.257	wt.%
O	Ka	224.24	9.469	26.213	wt.%
Fe	Ka	445.58	13.344	68.53	wt.%
				100.000	wt.%

3

Elt.	Line	Intensity (c/s)	Error 2-sig	Conc	Units
C	Ka	33.14	3.640	16.989	wt.%
Fe	Ka	587.89	15.331	83.011	wt.%
				100.000	wt.%

4

Figure 5: *Scanning electron microscopy and EDS analyses of the treated surface and edge of treated substrate where treated layer is removed (350V-5 minutes)*

A second SEM-EDS analysis was also performed on the cross-section, but before this operation the oxy-carburised layer on the edge of the sample was removed to find out the differences between treated surface morphology. Figure 5 shows the SEM image and results of elemental analysis corresponding with the rectangles. In Figure 5 rectangles 1 and 4 show that the treated and removed part of the substrate, and the tables show the elemental analyse results taken from related areas. In addition, to reveal the adverse effect of low voltage on PE, the surface of

the treated sample at 200 V was investigated by electron microscopy as shown in Figure 6. In Figure 6, Panel 1 shows the elemental analyse results collected from point 1, and Panel 2 shows the results collected from rectangle 2. Figure 6 may be considered to explain the mechanism of PE at low voltage stages. Panel 1 has pretty much C and O concentration than Panel 2. The current–voltage characteristics can explain a mechanism of partially carbo-oxidized areas during the plasma discharging. Several reviews about current–voltage characteristics of plasma electrolysis have been published. According to the current–voltage dependence under electrolytic plasma discharge, there are four types of stages of metal-electrolyte systems being discussed in literature [4, 11]. These are identified as gas liberation (U1), spark ignition (U2), continuous plasma envelope (U3), and arcing region (U4). Considering the sample treated at 200V, the V-I characteristic was in the range of the U1-U3 stages, and the continuous plasma envelope was not maintained constant because of the lower applied energy per unit area. This insufficient energy may have caused the localized melting and oxidation.

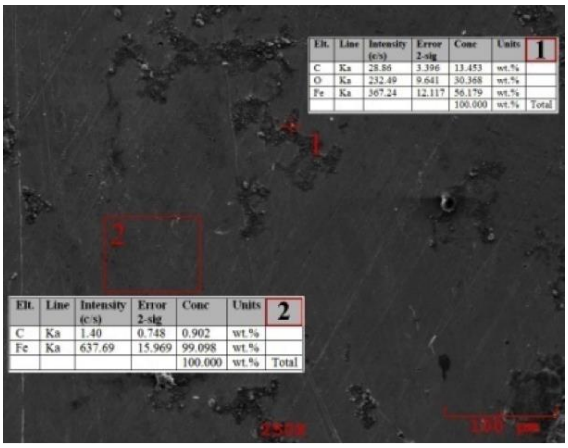

Figure 6: *Scanning electron microscopy and EDS analysis of the treated surface (200V-5 minutes)*

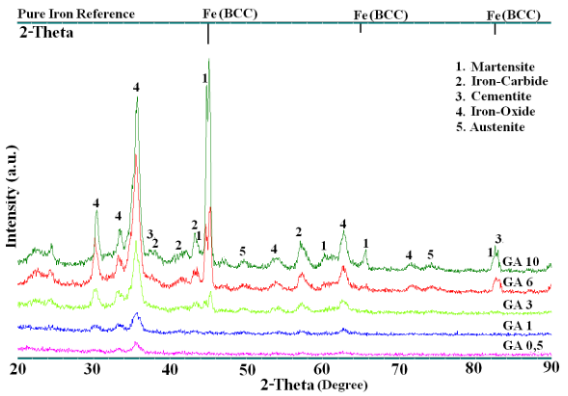

Figure 7: GA-XRD patterns of carburised pure iron at 0.5°, 1°, 3°, 6° and 10°, treated 5 minutes-300V

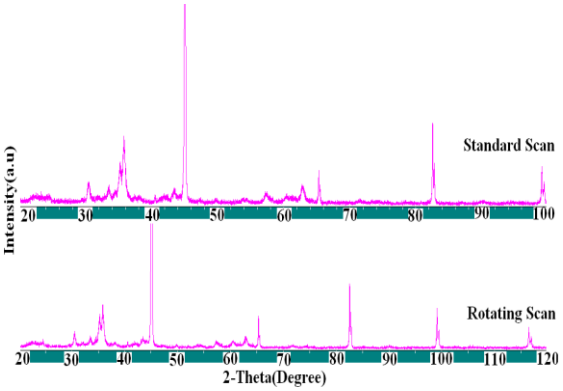

Figure 8: *Standard Scan-XRD(2theta 20-100) and Rotating Scan-XRD(2theta 20-120) patterns of carburised pure iron, treated 5 minutes-300V*

The mechanical performance of PE was evaluated by microhardness testing throughout the diffusion layer. The results are given in Figure 7 for each treatment parameter. Even at low voltages such as 200V, some slight increases were measured on the near surface of the treated layer; the hardness depth was not detected 10 μm beneath the surface. As the treatment voltage increased from 250 V to 350 V, depending on the increase in diffusion depth of carbon and oxygen, the microhardness and the depth of hardened zone increased. Due to high diffusion rate of C and then rapid cooling rates on the surface, [16] "from the austenite phase of the iron which is saturated with carbon atoms" [7], nanocrystalline structures [6, 11] and martensite phase, cementite, austenite [9] can form at the surface. The aforementioned phases are transformed from ferrite to austenite and subsequent quenching. They were identified by a series of XRD diffraction methods such as Glancing Angle (GA-XRD), which enables analysis of the thin layers on a treated surface without removing data from their substrate material; Rotating Scan (RS-XRD), which enables analysis of a rotating sample, giving information for all surfaces; and Standard Scan (SS-XRD). GA-XRD tests were performed at 0.5°, 1°, 3°, 6°, 10° and identified possible phases are shown in Figure 7. GA-XRD analysis of the carburised layer shows that the surface consists of a mixture of ironcarbide, martensite, cementite, and ironoxide. In addition, formation of ironcarbide, martensite, cementite, and ironoxide were detected by RS-XRD and RS-XRD (Figure 8). These formations such as martensite, ironcarbide or oxides lead to an increase in surface microhardness. The surface hardness of the pure iron was increased from the about 160-170 HV(25gf) to about 820 HV(25gf) after PE (Figure 9). Furthermore, the diffuse-type hardness profile regarding the engineering performance of work can be achieved in both surface properties (Hard) and mechanical properties of the core (Ductile) [17].

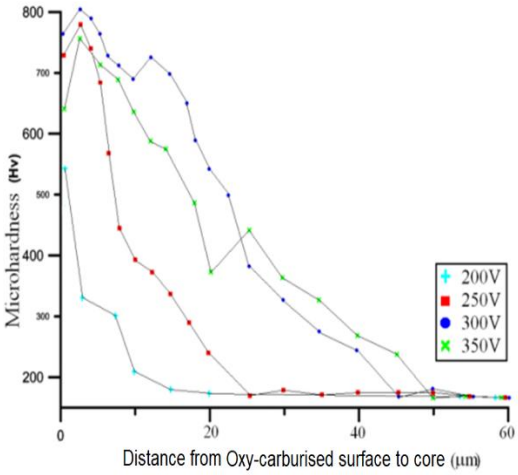

Figure 9: *Microhardness profiles for pure iron treated by PE for 5 minutes at 200, 250, 300 and 350V*

3.2. Wear and friction characterization

It is expected that oxy-carburised surface may present a better wear resistance relative to its high hardness value [4]. Figure 10 shows the variations of wear volume with applied normal loads (Figure 10a) and different sliding distances (Figure 10b) for the pure iron and carburised specimens tested under dry linear reciprocating against an AISI 52100 steel ball. With an increase in the load, the wear loss of pure iron and carburised pure iron presents an obviously different trend. It can be seen from Figure 10a that the wear loss of the untreated pure iron sample increases with an increasing normal load; however, this increasing rate is not directly proportional after a 10N load. It can be seen that at loads of 10N and 15N for pure iron, the wear loss does not show a remarkable increase, but considering the carburised sample it clearly increases. For pure iron, it is expected that severe wear parameters cause more removed and worn volume. However, as mentioned before, the wear loss of 15N is not much more than that of 10N. This may be explained by the oxide formation between sliding couples because the friction energy generates heat and plastic deformation on local contact surfaces during wear [18]. Regarding the carburised sample, as can be seen in Figure 10a, the volume loss of carburised pure iron is almost the same for 5N and 10N applied loads, and wear resistance is much greater compared to the wear loss of pure iron under the same loads. Interestingly, the carburised sample exhibited drastically high wear loss under the 15N load compared to the 5N and 10N loading conditions.

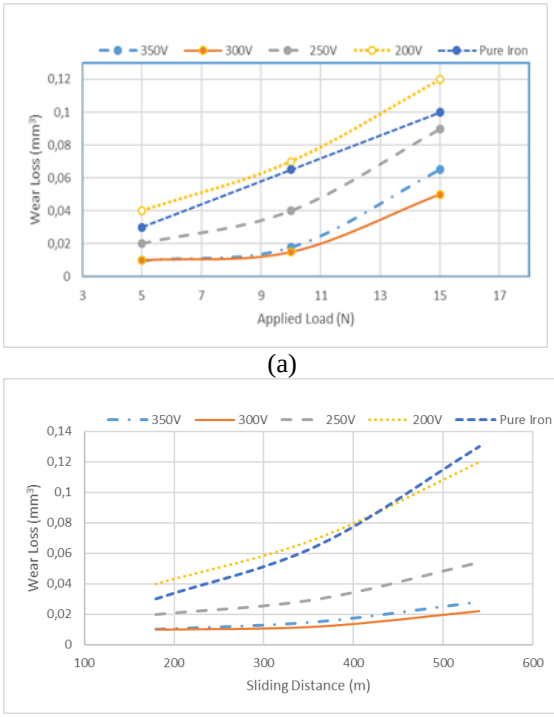

Figure 10*: Wear loss for carburised and pure iron specimens for different applied loads (a) and sliding distances (b)*

The wear loss is probably caused by relatively intensive hard carbide material dissolution or creation of oxide debris from both the sliding ball surface and the carburised layer. These hard particles may cause abrasive wear to the interior layer of the carburised sample where it is relatively softer and a less carbonized zone. Even the contact area may reach directly to the substrate under severe loads and long sliding distances [19]. Therefore, tribological conditions such as the friction coefficient and roughness may change during the wear test [20]. In addition, severe plastic deformation leads to the formation of a predominantly finer grains [21]. Grain refinement may affect the wear behaviour of sliding couples. On the other hand, plastic deformation is caused by the shear stress that arises at the point of contact due to adhesion and "plowing". It has been suggested that the depth of deformation increases with sliding distance and eventually reaches a steady state value [22]. With regards to the wear test of sliding distances of 180, 360, and 540 m under 5N, expected changes such as quasi-linear volume loss may take place during the wear test. There was no dramatic wear loss detected for the mentioned test. Oxy-carburising gave rise to a significant improvement in the wear resistance of treated specimens for the sliding distance-dependent wear tests (Figure 10a). The friction coefficients observed in reciprocating-sliding wear tests at 5, 10 and 15 N

normal loads, friction coefficients are given in Figure 11 and Table1. The higher initial friction coefficient onset of reciprocating is presumably because of the strong adhesion that is related with the smoothness of the initial surfaces of the pure iron and the 52100 steel ball. The friction coefficients of the oxy-carburised samples (under 10N load~ 0.4) were slightly lower than that of the substrate (10N ~0.6). Considering the effects of PE oxy-carburising treatments, it was noticed that despite of the sharp increase in surface roughness from 0.01 to 0.18 µm the average friction coefficient of the oxy-carburised samples was slightly lower than that of the pure iron. The sample treated at 300 V during 5 min. and 350 V 1 min. demonstrated a much higher wear resistance than both the untreated sample and those treated under different conditions, for which severe ploughing through the surface was observed.

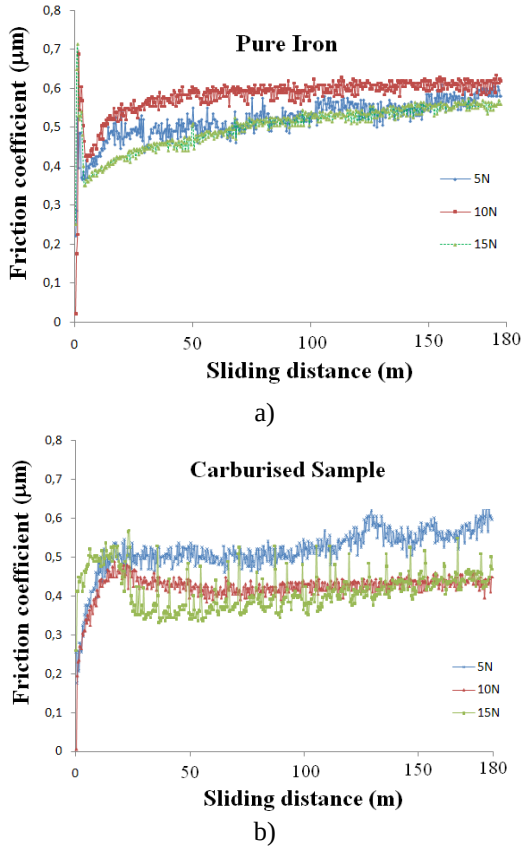

Figure 11: *Friction coefficients for reciprocating-sliding wear tests of the untreated substrate (pure iron) and carburised samples against AISI 52100 balls at 5, 10 and 15N normal loads and 180 m sliding distance.*

Typically, cathodic PE carburizing leads to increases in the surface roughness, but the surface hardness also increases owing to the formation of martensitic layer, providing improved wear resistance. On the other hand, Anodic PE carburizing usually results in surface smoothing and causes friction coefficient to decrease, but it is always accompanied by the formation of an oxide layer. In this case, an improvement in the wear resistance is not always associated with increased hardness, being determined by a combination of the hard martensitic sublayer and a porous oxide surface layer which can retain lubricants. Indeed, in this study, not only carburizing but also oxy-carburising, both carbide and oxide phases were formed together. This increases the hardness and wear resistance. Oxygen produced by the electrolyte circulation and produced by disintegration of H_2O_2 was continuously transferred to the plasma zone. The oxide and carbide phases formed on the surface are given in Figure 6 and 7.

Table 1. Plasma Electrolysis Parameters and Friction Coefficients (µ)

Load	Plasma Electrolysis Par. and Friction Coef				(µ)
	350V (5min)	300V (5 min)	250V (5min)	200V (5min)	Pure Iron
5 N	0,4	0,38	0,45	0,5	0,55
10 N	0,43	0,41	0,48	0,51	0,6
15 N	0,49	0,48	0,55	0,56	0,53
	350V (3min)	300V (3 min)	250V (3min)	200V (3min)	Pure Iron
5 N	0,38	0,4	0,45	0,51	0,55
10 N	0,42	0,43	0,5	0,52	0,6
15 N	0,48	0,49	0,55	0,54	0,53
	350V (1min)	300V (1 min)	250V (1min)	200V (1min)	Pure Iron
5 N	0,47	0,46	0,48	0,56	0,55
10 N	0,5	0,51	0,57	0,59	0,6
15 N	0,51	0,51	0,52	0,53	0,53

Figure 12 shows the SEM micrographs revealing the wear tracks and corresponding EDS analysis of the pure iron (a) under 5N, (b) under 10N and (c) 15N applied loads. Considering Figure 12a, the EDS spectra confirms a small scale oxidation (marked by 1 and 2), and cutting lines that occurred in the wear track along the sliding direction (marked by 3) showing the presence of abrasive wear mode. On the other hand, the worn surface shows less evidence of fracture or plastic deformation type wear characteristics. In Figure 12 the small rectangle presents the SEM image of wear scar of pure iron captured at lower magnification; this scar also presents a few narrow grooves formed by the ploughing action due to the abrasive particles and spalling pits formed by adhesive wear. Although the EDS analyses show the presence of C, this may have

originated from the sliding ball or sample preparation chemicals.

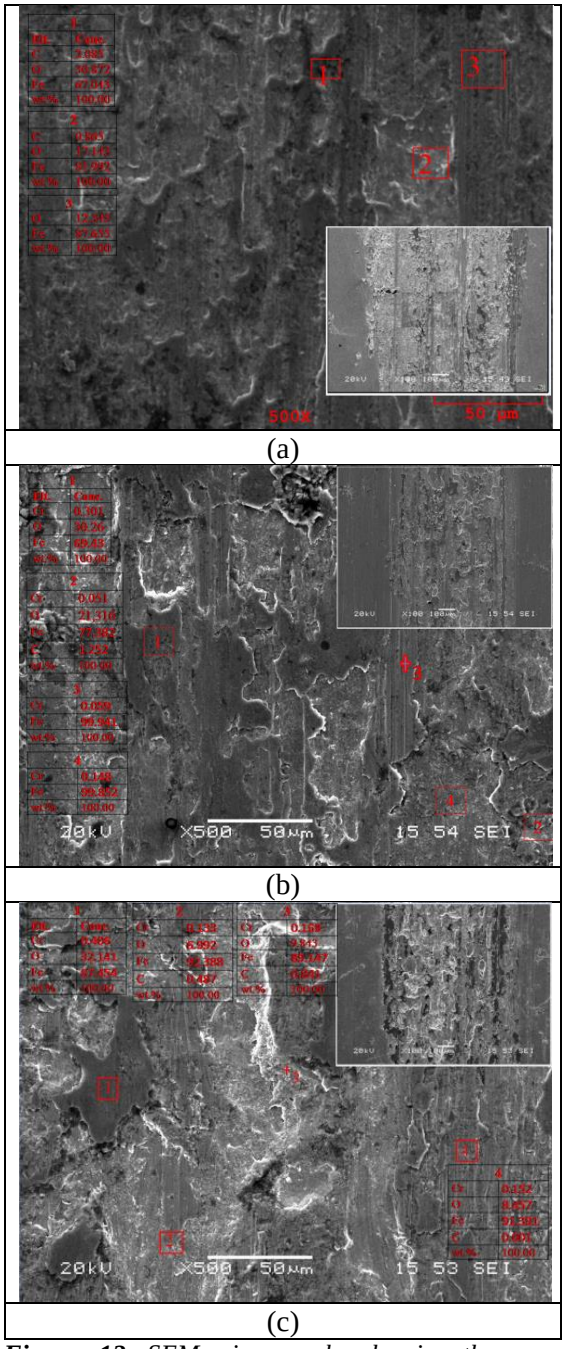

Figure. 12: *SEM micrographs showing the wear tracks and EDS analysis of the pure iron (a) under 5 N, (b) under 10N and (c) 15 N applied loads.*

As can be seen from Figure 12b, the worn surface is clearly different than Figure 12a and the wear loss of Figure 12b is twice as large as that in Figure 12a. During sliding, higher loads enhance the rate of fracture, and consequently larger amounts of wear take place [23]. As can be seen in Figure 12b, by increasing the applied load to 10 N, wear mechanisms show predominantly abrasive and oxidative wear behaviour. Parallel to these mechanisms, the EDS spectra proves the increasing oxidation level (marked by 1, 2). The EDS spectra marked by 1 shows the chemical composition of 30.26 wt.% oxygen, 69.43 wt.% iron, and 0.301 wt.% chromium that is taken from a flat layer adhered on (flake like formation) the plate or deformed-smoothened tips. A percentage of 30.26wt% O and 69.43wt% Fe detected by EDS may support the formation of iron oxides. Recent studies are in agreement with these formations of iron oxide such as Fe2O3, Fe3O4, and FeO depending on the rubbing temperature [23, 24]. Elemental material transfer is considered as a likely interaction between sliding couples [25]. The EDS spectra of remarkable areas with regard to wear characteristics in Figure 12b marked by 1, 2, 3, and 4 show the chromium transfer from one to another. Chromium transfer is related to several events such as thermomechanical and thermochemical mechanisms that occur at the interface of sliding contacts. At the inception of sliding, the surface morphology of these contacts is described as asperity-to-asperity mode, and later morphology changes as area-to-area. Formation of severely deformed and strained transfer patches are addressed as assumed reason for the chemical and/or mechanical alloying take place in [26]. With regards to the result of the alloying and oxidation mechanism, fine powder metallic iron particles may be formed [27]. Points 3 and 4 in Figure 12b show the presence of metallic iron and chromium. Tribo-electrification is described as a phenomenon that consists of electric charge, which is generated by abrasion between the relative motions of contacting surfaces. Evaluating the effect of tribo-electrification on wear conditions for steel pins sliding on the iron, whether the sliding contacts are charged with negative or positive polarity depends on the conditions [25, 28]. As a result, this polarization force causes material transfer, and that is why it is discussed in this study as a possible transfer mechanism. It is observed in Figure 12c that a higher load gives rise to a rough surface as a result of adhesive wear and material transfer. Discernible traces of adhesive craters, scratches from ploughing (around mark 3), depressions (rough white areas), flattened areas containing O and Fe (numbered as 1), a groove at the edge of the wear scar (small figure 100X magnified, and plastic deformations (around mark 4) can be observed all over the figure. All EDS marks indicate the presence of Cr and O. Detecting material transfer, especially Cr, in the large area may be explicated as an increase of wear loss of the bearing ball. It is worth mentioning here that we have attempted to measure microhardness of the worn scar on different areas to find evidence for the differences on the hardness depending on the strain hardening. For the pure iron, some brittle cracks

originating from strain hardening have been observed [29]. However, it was not possible to measure on uneven surfaces, but on the flattened surface marked by 1 in Figure 12c which consists of Cr 0.406, O 32.141, and 67.45 wt.%. Finally, the microhardness of the mentioned area was measured as 260 HV, which is higher than the initial microhardness (about 170 HV) of pure iron. First of all it should be mentioned that the increase of microhardness could be relative to the amount of load and deformation. Researchers have suggested that hardening near the sliding surface of pure iron is due to the very fine structure caused by severe plastic deformation. They have reported that the hardness of the ultra-fine structure layer is about two times harder than matrix [30]. On the other hand, the reason for this difference in the hardening behaviour could be oxide formation that is dispersed in iron matrix [31, 32]. In regard to the dispersion of particles in matrix, a new model called 'Equivalent Hardness' has been proposed to make the abrasion behaviour of iron-base alloys clear. The equivalent hardness (Heq) is calculated as follows:

$$H_{eq}=f_m x H_m+f_{hp}+H_{hp} \quad (1)$$

where f_m is the matrix volume fraction, f_{hp} the hard phase volume fraction, H_m the matrix hardness measured after the wear test, and H_{hp} the hard phase hardness. For our experiment, iron oxides and chromium may behave as hard phase and pure iron may behave as matrix [32].

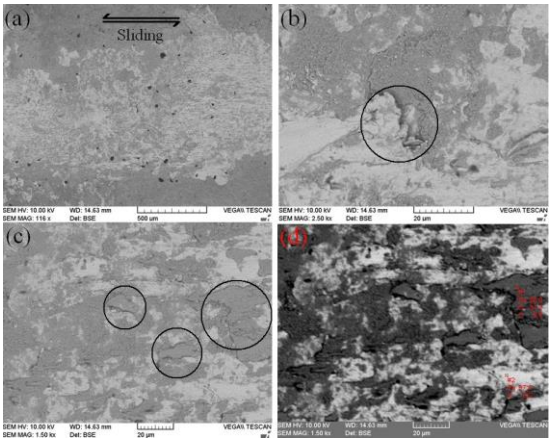

Figure 13: *SEM micrographs taken in different magnification modes showing the wear tracks of the carburised pure iron under 5N applied load.*

The wear scar microstructures of oxy-carburised iron under a 5N applied load and 180 m sliding distance for the several magnification levels of SEM-BSE images are illustrated in Figures 13, a, b, c and d (EDS). Thermochemical treatment is able to generate diffusion layers to enhance tribological properties. As previously mentioned, carburising, in which the surface layer is saturated with carbon content, and subsequent quenching and tempering to low temperatures increases the resistance to abrasion by hard particles [33]. Indeed, no significant wear loss and trace that is related with abrasion was detected in Figure 13 for all panels. According to the wear loss and SEM observations, it may be concluded that the carburised samples can withstand 5N contact stresses up to 540 m sliding distance and 10N contact stresses over a 180 m sliding distance. SEM-EDS analyses show the oxidation of carburised tips (panel d 1). On the other hand, no oxidation was observed from panel d marker 2: the EDS spectra detected only Fe-C elements.

Figure 14: *Surface profile of the carburised and polished pure iron before wear test*

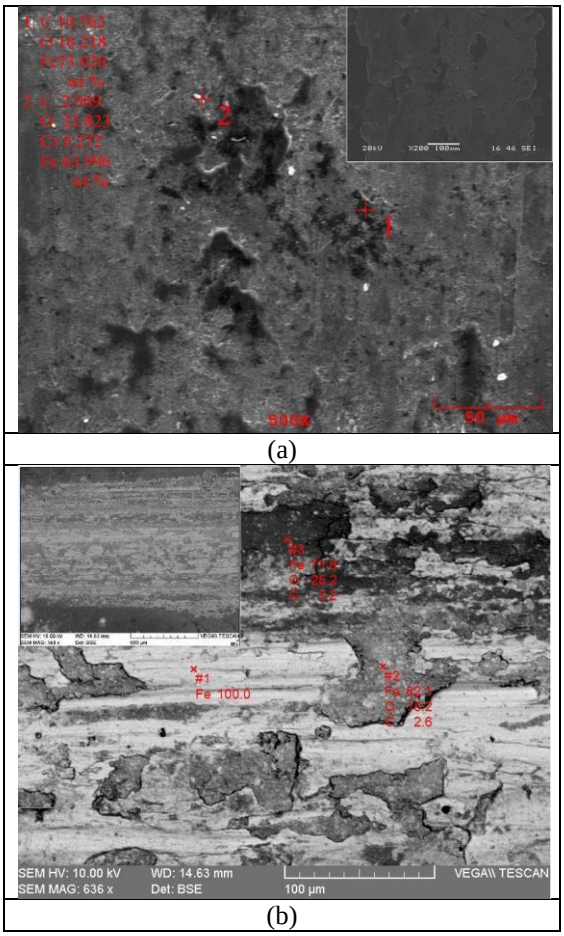

Figure 15: *SEM micrographs taken in different magnification modes showing the wear tracks and EDS analysis of the carburised pure iron under (a) 10N and (b) 15N applied loads.*

In order to evaluate the tribological behaviour of oxy-carburised samples the roughness characteristic of the oxy-carburised layer should be investigated. The effect of roughness parameters and friction on wear has been reported [34-36]. To gain a deeper insight into such wear mechanisms that are considered with surface asperities, the surface profile of oxy-carburised and that of polished pure iron were measured. A comprehensive surface profile of the oxy-carburised and polished pure iron graphs that are presented in Figure 14 shows that the oxy-carburised pure iron has a distinctly higher surface roughness and asperities than polished pure iron. The surface profile comparison also indicates that the plasma oxy-carburising increases the surface hardness when performing on a polished surface in the range of our process parameters of PE. In Figure 14, several tips on an oxy-carburised pure iron panel are marked by an X symbol. During the onset or middle period of sliding, these tips and sliding counter ball/pin contact each other. Consequently, higher local contact pressure, which is generated on the tips of the surface, leads to flattening and deformation of the asperities. Taking into account the surface profile and tips marked X, it may be concluded that the circles shown in Figure 13 show the flattened and slightly worn tips. These rough asperities and tips wear the steel ball faster than polished pure iron.

The apprehensible comparison between the low friction coefficient and low wear loss in this wear test is the oxy-carburised sample tested at a 10N load (Figure 15a), showing reduction in friction (Figure 11) and a wear loss, as compared to the pure iron at the same load and sliding distance. With regards to the low applied load, the oxy-carburised sample tested at a 5N load exhibited a nearly twice better wear resistance than pure iron (Figure 10). However, wear loss data of the oxy-carburised sample under relatively higher loads such as 10 and 15N gives dramatic results. Although the carburised layer under 10N shows the best wear resistance, the resistance of the same layer is significantly lower at 15N. Figure 15 shows the SEM microstructure of the worn scar of carburised samples tested at 10 and 15N. At the end of the wear test, as shown in Figure 15a, the carburised sample did not show any indication of failure for loads of 10N. The EDS spectra shows typical oxidation on some locations and Cr transfer from the bearing ball to oxy-carburised layer whereas at 15N, SEM micrographs show some signs of failure in terms of adhesive transfer, abrasive/adhesive wear, flattened areas, and embedded particles in the wear scar (Figure 15b). Unfortunately, at 15N, the carburised layer did not show adequate wear resistance and the wear resistance was weaker even than untreated polished iron. It can be claimed that a carbon diffusion layer consisting of hard phases such as martensite and cementite cannot supply the necessary load bearing capacity at 15N. The cumulative effect of higher surface roughness and heavier applied loads gives rise to an increase on the contact areas which is why the carburised layer fails at 15N. Failed particles or small intricate layers, which are mainly compounds of hard carbide and oxides, wear and then stick the ball, whilst at the same time the ball causes gouging from the hard surface to soft interior of the diffusion layer. When the carburised layer has been gradually worn into the core the ball makes contact with the less carburised and relatively softer layer. These contacts between the ball and the softer new layer causes the severe wear rate due to the abrasive effect of the adhered particles agglutinated to the ball, hard debris (causing third body effect), and adhesion between couples.

3.3- Corrosion behaviour

The corrosion resistance characteristics of the specimens are investigated by electrochemical tests such as the potentiodynamic polarisation test (PDT), open circuit potential (OCP), and electrochemical impedance spectroscopy (EIS).

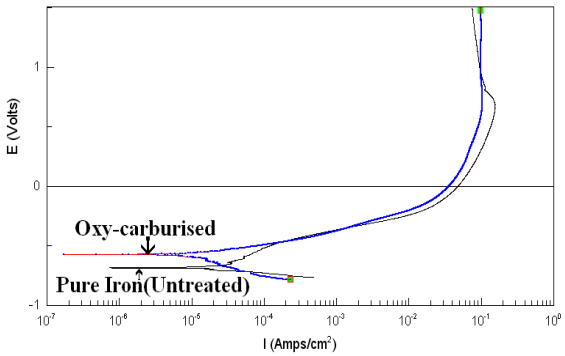

Figure 16: *Potentiodynamic corrosion scans of the oxy-carburised at 300V-5minutes and the untreated pure iron*

Figure 16 shows the potentiodynamic polarisation scans of the oxy-carburised at 300 V-5 minutes and the untreated pure iron substrates in the aerated solution of 3.5%NaCl at room temperature. The potential of the oxy-carburised samples is nobler than the untreated pure iron substrate. As can be seen in potentiodynamic curves (Figure 16), the corrosion potential (Ecorr) of the sample oxy-carburised at 300V is -0.57 V and the corrosion current density (Icorr) is 1,228E-5(Amps/cm2). Controversially, the PDT result of the untreated substrate was found to be Ecorr = -0.68 V and Icorr 2.736 E-5(Amps/cm2). It can be seen that the sample treated at 300 V has a

lower value of corrosion current (Icorr) and a more positive corrosion potential (Ecorr) compared to the untreated substrate, and this indicates an enhancement in corrosion resistance.The values of the cathodic (βc) and anodic (βa) Tafel slopes, and polarization resistance (Rp) at the corrosion potential are measured from the potentiodynamic polarization scan by the corrosion software, CorrView, according to the well-known Stern–Geary equation [37, 38].

The Rp value is calculated as follows,

$$Rp=B/Icorr \quad (2)$$

Here, B is a constant that is calculated from the anodic and cathodic Tafel slopes as follows,

$$B=(\beta c.\beta a)/(2.3(\beta c+\beta a)) \quad (3)$$

While the Rp value of the oxy-carburised layer was 1447 ohms/cm2, the Rp value of the pure iron layer was 751 ohms/cm2. According to the Rp values, after PE the polarisation resistance slightly increased, which is probably due to the formation of the oxy-carburised layer on the surface. SEM images showing the surface state of the oxy-carburised and pure iron substrates after corrosion testing are shown in Figures 17a and 17b respectively. Figure 17 confirms that the oxy-carburised layer formed at 300 V slightly prevents the pitting corrosion attack by acting as a barrier to protect the material substrate from the reaction with the NaCl solution, but on the other hand, many large pits and crevices can be easily seen on the pure iron substrate.

In addition to the corrosion tests, EIS was carried out to explore the numerous advantages of this technique in the evaluation of electrochemical mechanisms underlying corrosion behaviour of engineered surfaces [39, 40, 41].

In this method, Bode and Nyquist plots are used, in particular to evaluate the behaviour of the corrosion process in comparison with other electrochemical techniques. The EIS results, in the forms of both Nyquist and Bode (amplitude and phase angle) plots, are presented in Figure 18. For the pure iron and oxy-carburised samples, EIS shows two steps: the first as the high-frequency part arises from the ohmic resistance due to the electrolyte and the impedance characteristics resulting from the penetration of the electrolyte through a porous film; and the second is the low-frequency part accounting for the processes taking place at the treated layer/electrolyte interface. The Nyquist plot and Bode plots show that the corrosion resistance increased by applying the oxy-carburising.

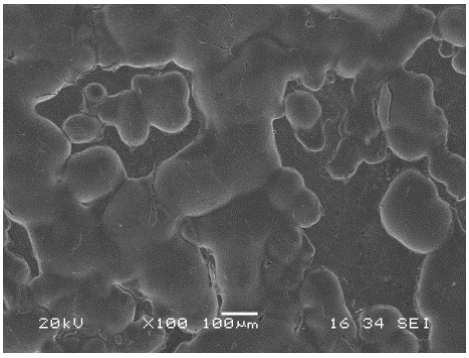

(a)

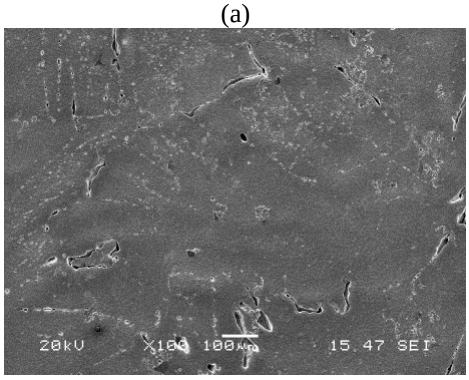

(b)

Figure 17: *SEM images showing the surface state of the oxy-carburised (a) and pure iron (b) substrates after electrochemical corrosion tests*

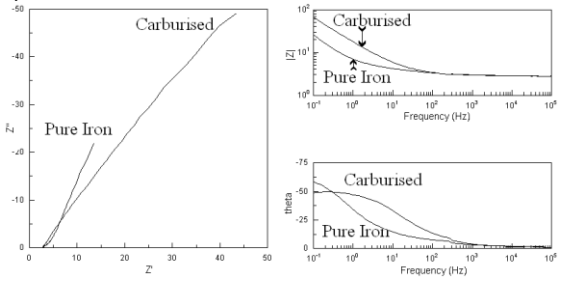

Figure 18: *EIS results (Nyquist plot is to the left and Bode-phase diagrams are to the right) for the samples of (oxy-carburised) treated and untreated pure iron*

The equivalent circuit modelling of EIS data is used to extract physically meaningful properties of the electrochemical system by modelling the impedance data in terms of an electrical circuit composed of ideal resistors (R), capacitors (C), and inductors (L). In the equivalent circuit analogue, resistors represent conductive pathways for ion-electron transfer and the resistance to the charge-transfer process at the electrode surface [42]. Capacitors and inductors are associated with space-charge polarization regions, such as the electrochemical double layer, and adsorption/desorption processes at an electrode. To address surface inhomogeneity, capacitances in equivalent circuits employed to fit EIS data are usually replaced with constant phase elements

(CPEs). As the electrode surface is coarse, a 'scattering effect' is often observed, i.e. the capacitance becomes a distributed parameter that means the electrochemical response in some sites deviates from the lump capacitance. The impedance for the constant phase element is discussed elsewhere [43, 44].

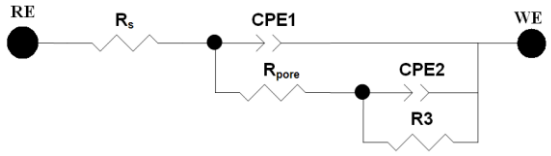

Figure 19: *Equivalent circuit proposed for simulation of the impedance behaviour of oxy-carburised layer*

Conclusion

Plasma electrolysis has been performed on pure iron substrate to obtain an oxy-carbon diffusion layer in a very short time in an aqueous sodium carbonate, H2O2 and glycerine electrolyte. A Novel PE system was designed to provide plasma stability and temperature control with 5 °C precision. Sample temperatures were also measured when PE was applied.

The process duration and applied voltage of the PE ranged from 1 to 5 minutes and from 200 to 350 V. The optimum oxy-carburising parameter was designated as 5 minutes-300 V because of the surface characteristic, glow discharge behaviour in a steady state regime, homogeneity of oxy-carbon layer, and microhardness. An oxy-carburised layer of ~30 μm case depth was formed at the surface during the treatment at 300V for 5 minutes and the hardness of the pure iron was increased from about 160-170 HV(25gf) to about 820 HV(25gf) by PE.

The oxy-carburised hard layer, which consists of multi-phase combinations of carbo-oxides, including mixtures of (Fe)2-3O3-4, austenite, martensite, and (Fe)xC, improved the wear resistance of pure iron in the linearly reciprocating ball-on-plate sliding condition up to a 10N load: once this limit was surpassed, the wear rate increased drastically. The wear mechanism was mainly affected by abrasive particles fractured from the oxy-carburised layer and adhesion at a 15N load.

It was measured that the friction coefficients of the oxy-carburised samples (at 10N load~ 0.4) were slightly lower than that of the pure iron (10N ~0.6).

A more positive corrosion potential, lower corrosion current and increased polarisation resistance were recorded for oxy-carburised layers, compared to pure iron.

References

[1] W. Gräfen, B. Edenhofer, Surface & Coatings Technology 200 (2005) 1830–1836
[2] Heat Treating, Volume 4 of the ASM Handbook
[3] M. Aliofkhazrae, A. S. Rouhaghdam, T. Shahrabi, Journal of Alloys and Compounds 460 (2008) 614–618
[4] A.L. Yerokhin et al. Surface and Coatings Technology, Volume 122, Issues 2-3, 15 December 1999, Pages 73-93
[5] T. Paulmier, J.M. Bell, P.M. Fredericks, Thin Solid Films 515 (2007) 2926–2934
[6] M. Yaghmazadeh, C. Dehghanian, Plasma Process. Polym. 2009, 6, S168–S172
[7] L. C. Kumruoğlu, A. Özel, Materials and Manufacturing Processes, Volume 25, Issue 9 September 2010, pages 923 – 931
[8] S.F. Luk, T.P. Leung, W.S. Miu, and I. Pashby, Materials Characterization 42 65–71 (1999)
[9] M. Tarakci, K. Korkmaz, Y. Gencer, M. Usta, Surface and Coatings Technology, Volume 199, Issues 2-3, 22 September 2005, Pages 205-212
[10] C.C.R.S. Rossia et al. Int. Journal of hydrogen energy 34(2009)323–332
[11] E.I. Meletis, X. Nie, F.L. Wang, J.C. Jiang, Surface and Coatings Technology 150 (2002) 246–256
[12] T.Mizuno et al, Jpn. J. Appl. Phys. Vol. 39 (2000) pp. 6055-6061
[13] Standard test method for linearly reciprocating ball-on-flat sliding wear designation: ASTM International, G133-05.
[14] ASTM G61 - 86(2009) Standard Test Method for Conducting Cyclic Potentiodynamic Polarization Measurements for Localized Corrosion Susceptibility of Iron, Nickel, or Cobalt-Based Alloys
[15] Electro Plating US Patent- US 7,166,206 B2
[16] C. Cionea, PhD thesis, The University of Texas At Arlington, May 2010
[17] Y. Sun et. al. Wear 253 (2002) 689–693
[18] Y. Wang, T. Lei, J. Liu, Wear 231 (1999. 12–19
[19] G. Pantazopoulos et al. Surface & Coatings Technology 187 (2004) 77– 85
[20] X. Nie et al. Surface and Coatings Technology 139-2001.135142
[21] S. Descartesa, C. Desrayaudb, E.F. Rauch, Materials Science and Engineering A 528 (2011) 3666–3675
[22] www.dtic.mil (The delamination theory of wear, Nam P. Sub et. Al, September 1974 (MIT)
[23] M. Reza Bateni, J.A. Szpunar , X. Wang, D.Y. Li, Wear 260 (2006) 116–122
[24] J. Qu, P. J. Blau, B. C. Jolly, Wear 263 (2007) 719–726
[25] Y-P Changa, H-M Chu, H-M Chou, Wear 262 (2007) 112–120
[26] B.K. Prasad, Wear 260 (2006) 1333–1341
[27] M.D. Bermúdez, P. Iglesias, A.E. Jiménez, G. M-Nicolás, Wear 267 (2009) 1784–1790
[28] Y-C Chiou, Y-P Chang, R-T Lee, Wear 254 (2003) 606–615
[29] X. Jincheng, J. Caixia, G. Meizheng, W. Tianmin, Wear 217 (1998) I10-116

[30] H. Kato, M Sasase, N. Suiya, Tribology International43 (2010)925–928
[31] V.A. Shabashov et al. Materials Science and Engineering A361 (2003) 136–146
[32] Kassim S. Al-Rubaie, Wear 243 (2000) 92–100
[33] J. Suchánek, V. Kuklík, Wear 267 (2009) 2100–2108
[34] Jiaren Jiang, R.D. Arnell, Wear 239 (2000) 1–9
[35] M. Sedlacek, B. Podgornik, J. Vizintin, Wear 266 (2009) 482–487
[36] B. Hwang, S. Lee, J. Ahn, Materials Science and Engineering A335 (2002) 268–280
[37] K. Marušić, H. Otmačić, D. Landek, F. Cajner, E. Stupnišek-Lisac, Surface & Coatings Technology 201 (2006) 3415–3421
[38] El-Sayed M. Sherif, R.M. Erasmus, J.D. Comins, Electrochimica Acta 55 (2010) 3657–3663
[39] S. Ningshen et al. Corrosion Science 48 (2006) 1106–1121
[40] A. S. Hamdy et al. Int. J. Electrochem. Sci., 1(2006)171-180
[41] C. Liu, Q. Bi, A. Leyland, A. Matthews, Corrosion Science 45 (2003) 1257–1273
[42] Electrochemical Impedance Spectroscopy (EIS): Scribner Associates - Tutorial
[43] Y. Wang et al. Surface & Coatings Technology 204 (2010) 1685–1688
[44] N.M. Alanazi et al. Surface & Coatings Technology 205 (2010) 1750–1756